The development of a hybrid prediction tool for railway induced vibration

P. Bouvet [1], **B. Nélain** [1], **D. Thompson** [2], **E. Ntotsios** [2], **A. Nuber** [3], **B. Fröhling** [3], **F. Seyfaddini** [4], **G. Herremans** [4], **P. Reumers** [4], **G. Lombaert** [4], **G. Degrande** [4]
[1] Vibratec,
28 Chemin du petit bois, F-69131, Ecully, France

[2] University of Southampton, ISVR,
Highfield, Southampton SO17 1BJ, United Kingdom

[3] Wölfel Engineering GmbH + Co. KG,
Max-Planck Strasse 15, D-97204 Höchberg, Germany

[4] KU Leuven, Department of Civil Engineering,
Kasteelpark Arenberg 40, B-3001 Leuven, Belgium
e-mail: **geert.degrande@kuleuven.be**

Abstract
One of the main objectives of the SILVARSTAR project is to develop a user-friendly frequency-based hybrid prediction tool to assess the environmental impact of railway induced vibration. This model will be integrated in the existing noise mapping software IMMI. Following modern vibration standards and guidelines, the vibration level in a building in each frequency band is expressed as the sum (in decibels) of source, propagation and receiver terms. Each term can be determined experimentally or predicted with numerical models, resulting in a hybrid prediction model that provides increased flexibility and applicability. This paper focuses on the assessment of several modelling assumptions made in the prediction tool, as well as the validation of the computational core by comparing results with those obtained with state-of-the-art prediction models for several numerical case histories. Furthermore, measured transfer functions and train passages at a site in Lincent (Belgium) are used for experimental validation of the prediction tool, and to show its capability for hybrid predictions.

1 Introduction

Although rail is a sustainable and climate-friendly mode of transport, noise and vibration remain particular environmental concerns. People living near railways are becoming increasingly sensitive to high levels of noise and vibration, while the operation of sensitive equipment is hampered by high vibration levels. SILVARSTAR [1] is a two-year collaborative project under the Shift2Rail Joint Undertaking that aims to develop validated software tools and methodologies to assess the noise and vibration environmental impact of railway traffic. One of the objectives is to provide the railway community with a commonly accepted, practical and validated methodology and a user-friendly prediction tool for vibration. This tool will be used for environmental impact assessment of new or upgraded railways on a system level.

The prediction tool consists of an efficient computational core, supplemented with an extensive numerical and experimental database. The numerical database includes pre-computed soil impedance and transfer functions for various soil profiles (determined at sites across Europe) and track widths ranging from 3 m up to 12 m. This allows for a significant reduction of the calculation time. The experimental database includes measured transfer functions and train passages at various European sites, and can also be extended by the

user. The numerical predictions and experimental data are used in a hybrid framework, in which the vibration level is expressed as the sum (in decibels) of a source, propagation and receiver term.

This paper is organized as follows. Section 2 presents the general framework for the prediction tool involving fully numerical, fully experimental and hybrid prediction schemes. In section 3, the computational core of the prediction tool is validated numerically by comparing predictions for a nominal IC train running on a ballasted track (various soil types and train speeds) to results obtained with the state-of-the-art model TRAFFIC [2]. An experimental validation is performed in section 4 using measured data at a site in Lincent (Belgium). The hybrid prediction schemes are also demonstrated for this site. Section 5 demonstrates the hybrid prediction schemes implemented in the tool. Section 6 concludes the paper.

2 Methodology

2.1 General framework

The basic concept for the prediction of ground vibration in SILVARSTAR is to develop a frequency-based hybrid vibration prediction tool, following the general framework recommended in the ISO 14837-1:2005 standard [3]. This expresses the vibration level $A(f)$ in a building during a train passage as the product of a source term $S(f)$ for the vehicle-track interaction, a propagation term $P(f)$ for the soil and a receiver term $R(f)$ for the building:

$$A(f) \quad = \quad S(f)P(f)R(f) \tag{1}$$

or, equivalently, as a sum of terms in decibels. Equation (1) obtains the vibration level $A(f)$ by a product of three terms evaluated at the same frequency f, omitting the Doppler effect due to moving loads. However, this assumption gives reasonable results if the train speed is relatively low compared with the wave velocities in the soil, while maintaining low calculation times [4]. Each of the terms in equation (1) can be represented by numerical predictions or by experimental data.

2.2 Fully empirical prediction scheme

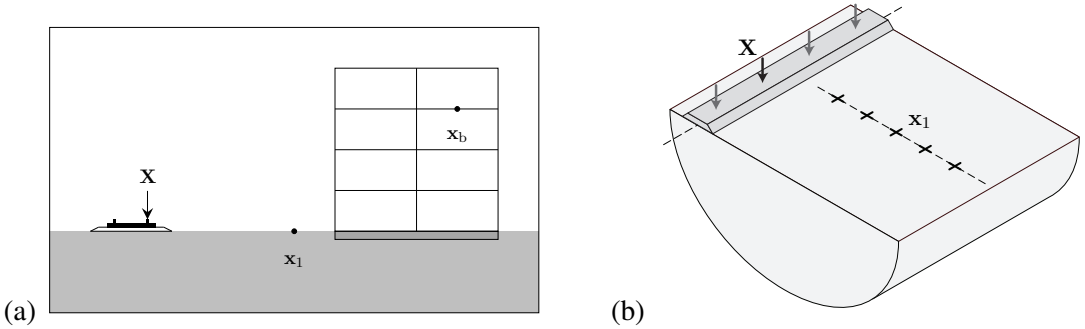

(a) (b)

Figure 1: (a) Source and receiver points for the FRA procedure and (b) excitation and receiver locations for line source transfer mobility measurements.

The empirical procedure for Detailed Vibration Assessment proposed by the Federal Railroad Administration (FRA) and the Federal Transit Administration (FTA) of the U.S. Department of Transportation [5, 6] conforms to the general framework recommended in ISO 14837-1:2005 and is used as a basis for the development of a hybrid vibration prediction tool. The vibration velocity level $\mathrm{L_v}(\mathbf{x}_\mathrm{b})$ at a receiver $\mathbf{x}_\mathrm{b}$ in the building (figure 1a) is defined as the root mean square value of the velocity during the stationary part of a train passage; it is expressed in decibels ($\mathrm{dB\ ref}\ 5 \times 10^{-8}\ \mathrm{m/s}$) in one-third octave bands as a sum of source, propagation and receiver terms:

$$\mathrm{L_v}(\mathbf{x}_\mathrm{b}) \quad = \quad \mathrm{L_F}(\mathbf{X}, \mathbf{x}_1) + \mathrm{TM_L}(\mathbf{X}, \mathbf{x}_1) + \mathrm{C_b}(\mathbf{x}_1, \mathbf{x}_\mathrm{b}) \tag{2}$$

$\mathrm{L_F}(\mathbf{X}, \mathbf{x}_1)$ is the equivalent force density ($\mathrm{dB\,ref.\,1N/\sqrt{m}}$). The vector $\mathbf{X}$ collects all source points on the rail heads, while the receivers $\mathbf{x}_1$ are located on the ground surface.

The line source transfer mobility $\mathrm{TM_L}(\mathbf{X}, \mathbf{x}_1)$ ($\mathrm{dB\,ref.\,5 \times 10^{-8} \frac{m/s}{N/\sqrt{m}}}$) is a measure for the vibration transmitted through the soil relative to the force density. It is derived from the superposition of point source transfer mobilities $\mathrm{TM_P}(\mathbf{X}_k, \mathbf{x}_1)$ for a series of n equidistant source points $\mathbf{X}_k$ with spacing h (figure 1b):

$$\mathrm{TM_L}(\mathbf{X}, \mathbf{x}_1) \quad = \quad 10 \log_{10} \left[h \sum_{k=1}^{n} 10^{\frac{\mathrm{TM_P}(\mathbf{X}_k, \mathbf{x}_1)}{10}} \right] \tag{3}$$

The force density $\mathrm{L_F}(\mathbf{X}, \mathbf{x}_1)$ is determined indirectly from the vibration velocity level $\mathrm{L_v}(\mathbf{x}_1)$ and the line source transfer mobility $\mathrm{TM_L}(\mathbf{X}, \mathbf{x}_1)$ by rearranging equation (2) and omitting the building correction factor $\mathrm{C_b}(\mathbf{x}_1, \mathbf{x}_\mathrm{b})$:

$$\mathrm{L_F}(\mathbf{X}, \mathbf{x}_1) \quad = \quad \mathrm{L_v}(\mathbf{x}_1) - \mathrm{TM_L}(\mathbf{X}, \mathbf{x}_1) \tag{4}$$

The receiver term or building correction factor $\mathrm{C_b}(\mathbf{x}_1, \mathbf{x}_\mathrm{b})$ can be quantified as a difference in vibration velocity level $\mathrm{L_v}(\mathbf{x}_\mathrm{b})$ at a point $\mathbf{x}_\mathrm{b}$ in the building, and $\mathrm{L_v}(\mathbf{x}_1)$ at a point $\mathbf{x}_1$ on the ground surface with the building present (figure 1a):

$$\mathrm{C_b}(\mathbf{x}_1, \mathbf{x}_\mathrm{b}) \quad = \quad \mathrm{L_v}(\mathbf{x}_\mathrm{b}) - \mathrm{L_v}(\mathbf{x}_1) \tag{5}$$

The vibration velocity levels can either be determined by measurements during a train passage, or calculated with a train-track-soil-building model. They can also be computed as a combination of adjustment factors to account for soil-structure interaction at foundation level and attenuation and amplification within the building; in SILVARSTAR, a combination of adjustment factors from the RIVAS project [7] will be used.

The source can also be characterized by a vibration velocity level $\mathrm{L_v}(\mathbf{x}_\mathrm{ref})$ at a reference distance $\mathbf{x}_\mathrm{ref}$ (e.g. 8 m or 25 m [8]). When equation (2) is evaluated for $\mathrm{L_v}(\mathbf{x}_1)$ and $\mathrm{L_v}(\mathbf{x}_\mathrm{ref})$, the former can be expressed as:

$$\mathrm{L_v}(\mathbf{x}_1) \quad = \quad \mathrm{L_v}(\mathbf{x}_\mathrm{ref}) + \mathrm{L_F}(\mathbf{X}, \mathbf{x}_1) - \mathrm{L_F}(\mathbf{X}, \mathbf{x}_\mathrm{ref}) + \mathrm{TM_L}(\mathbf{X}, \mathbf{x}_1) - \mathrm{TM_L}(\mathbf{X}, \mathbf{x}_\mathrm{ref}) \tag{6}$$

If it is assumed that the force densities $\mathrm{L_F}(\mathbf{X}, \mathbf{x}_\mathrm{ref})$ and $\mathrm{L_F}(\mathbf{X}, \mathbf{x}_1)$ are equal, equation (6) is approximated as:

$$\mathrm{L_v}(\mathbf{x}_1) \quad \simeq \quad \mathrm{L_v}(\mathbf{x}_\mathrm{ref}) + \underline{\mathrm{TM_L}(\mathbf{X}, \mathbf{x}_1) - \mathrm{TM_L}(\mathbf{X}, \mathbf{x}_\mathrm{ref})} \tag{7}$$

The underlined term represents the difference in line source transfer mobilities at the receivers $\mathbf{x}_1$ and $\mathbf{x}_\mathrm{ref}$, for excitation at source locations $\mathbf{X}$.

2.3 Fully numerical prediction scheme using a modular approach

A semi-analytical train-track-soil interaction model (based on GroundVIB [9]) is integrated in the prediction tool to compute the dynamic axle loads and forces transmitted to the ground. The vehicle is represented by a multi-body model (e.g. a 10-DOF model, figure 2a). The ballasted or slab track (figure 2b) is modelled by Euler-Bernoulli beams for the rail (and slab) with resilient layers for rail pads, under-sleeper pads, ballast and slab mat. Vehicle and track properties can be selected from a database or entered as numerical values.

The track is coupled to the soil over a finite width (figure 2c). The soil is represented by impedances in the frequency-wavenumber domain that are pre-computed for a range of track widths and soil properties (homogeneous and layered soils) using the state-of-the-art models MOTIV [10, 11] and TRAFFIC [2]. The train-track-soil interaction problem is solved in the frequency domain, considering the excitation due to rail and wheel unevenness. The force transmitted to the subgrade is then estimated in the wavenumber-frequency domain and the free field ground response is calculated using pre-computed soil transfer functions. The response due to a train passage is obtained by summation of the contribution of each axle. The response of the building is estimated as in the empirical prediction scheme by means of building correction factors [7].

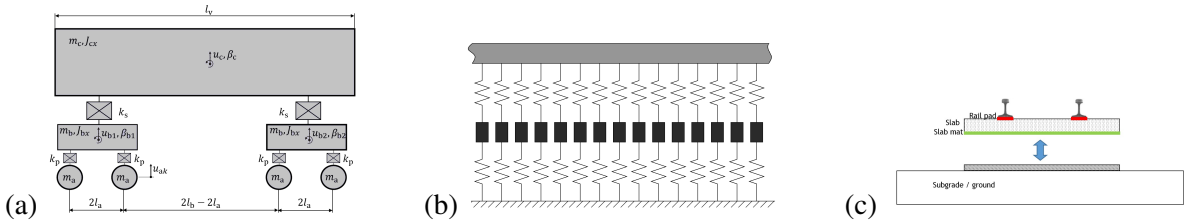

Figure 2: (a) 10-DOF vehicle model, (b) ballasted track model and (c) floating slab track on homogeneous soil.

2.4 Hybrid prediction schemes

Hybrid prediction schemes, in which numerical and empirical data are combined following equation (2), are also available, providing more flexibity and applicability than purely experimental or numerical models.

In hybrid model 1, a numerical source model is combined with an empirical propagation term $\mathrm{TM}_{\mathrm{L}}^{\mathrm{EXP}}(\mathbf{X}, \mathbf{x}_1)$ to predict the vibration level $\mathrm{L}_{\mathrm{v}}^{\mathrm{HYB}}(\mathbf{x}_1)$:

$$\mathrm{L}_{\mathrm{v}}^{\mathrm{HYB}}(\mathbf{x}_1) = \mathrm{L}_{\mathrm{F}}^{\mathrm{NUM}}(\mathbf{X}) + \mathrm{TM}_{\mathrm{L}}^{\mathrm{EXP}}(\mathbf{X}, \mathbf{x}_1) \tag{8}$$

The force density $\mathrm{L}_{\mathrm{F}}^{\mathrm{NUM}}(\mathbf{X})$ can be computed directly from the dynamic axle loads, or alternatively, as the difference between a predicted vibration velocity level $\mathrm{L}_{\mathrm{v}}^{\mathrm{NUM}}(\mathbf{x}_1)$ and line source transfer mobility $\mathrm{TM}_{\mathrm{L}}^{\mathrm{NUM}}(\mathbf{X}, \mathbf{x}_1)$:

$$\mathrm{L}_{\mathrm{v}}^{\mathrm{HYB}}(\mathbf{x}_1) = \mathrm{L}_{\mathrm{v}}^{\mathrm{NUM}}(\mathbf{x}_1) \underline{- \mathrm{TM}_{\mathrm{L}}^{\mathrm{NUM}}(\mathbf{X}, \mathbf{x}_1) + \mathrm{TM}_{\mathrm{L}}^{\mathrm{EXP}}(\mathbf{X}, \mathbf{x}_1)} \tag{9}$$

The underlined term can be interpreted as a correction term on the predicted vibration velocity level, accounting for the difference between the measured and predicted line source transfer mobility. Equations (8) and (9) are particularly useful to assess new rolling stock or a new railway line.

In hybrid model 2, a measured force density is combined with a predicted line source transfer mobility:

$$\mathrm{L}_{\mathrm{v}}^{\mathrm{HYB}}(\mathbf{x}_1) = \mathrm{L}_{\mathrm{F}}^{\mathrm{EXP}}(\mathbf{X}, \mathbf{x}_1) + \mathrm{TM}_{\mathrm{L}}^{\mathrm{NUM}}(\mathbf{X}, \mathbf{x}_1) \tag{10}$$

$$= \mathrm{L}_{\mathrm{v}}^{\mathrm{EXP}}(\mathbf{x}_1) \underline{- \mathrm{TM}_{\mathrm{L}}^{\mathrm{EXP}}(\mathbf{X}, \mathbf{x}_1) + \mathrm{TM}_{\mathrm{L}}^{\mathrm{NUM}}(\mathbf{X}, \mathbf{x}_1)} \tag{11}$$

which is useful to assess mitigation measures in the transmission path.

In all previous expressions, the building correction factor $\mathrm{C}_{\mathrm{b}}(\mathbf{x}_1, \mathbf{x}_{\mathrm{b}})$ was omitted for brevity. When assessing vibration in a new building close to an existing railway, for example, the following hybrid approach can be employed:

$$\mathrm{L}_{\mathrm{v}}^{\mathrm{HYB}}(\mathbf{x}_{\mathrm{b}}) = \mathrm{L}_{\mathrm{F}}^{\mathrm{EXP}}(\mathbf{X}, \mathbf{x}_1) + \mathrm{TM}_{\mathrm{L}}^{\mathrm{EXP}}(\mathbf{X}, \mathbf{x}_1) + \mathrm{C}_{\mathrm{b}}^{\mathrm{NUM}}(\mathbf{x}_1, \mathbf{x}_{\mathrm{b}}) \tag{12}$$

while in case of an existing building next to a new-built railway, an empirical building correction factor $\mathrm{C}_{\mathrm{b}}^{\mathrm{EXP}}(\mathbf{x}_1, \mathbf{x}_{\mathrm{b}})$ can be added to equations (8) or (9).

2.5 Implementation of the hybrid prediction tool

The prediction model is developed based on the GroundVIB model [9], which uses 2.5D models for the track and the soil [12]. Various assumptions (see section 3.1) are made in the prediction model to speed up computations. The model is integrated into the existing noise mapping software IMMI, developed by Wölfel, and is linked to a Geographical Information System (GIS), providing a software platform with Graphical User Interfaces (GUIs) that will allow engineers to perform noise and vibration environmental impact studies within the same integrated environment.

The use of pre-computed soil impedance and transfer functions from a numerical database [13] considerably speeds up calculations and allows the user to assess in real-time the effect of changes in train, track and soil

parameters on axle loads and vibration. The pre-computed data are available for various homogeneous and layered soils, and track widths ranging from 3 m up to 12 m.

An experimental database [13] contains force densities, line source transfer mobilities, free field vibration velocity levels, and corresponding train, track, unevenness and soil properties from well-documented measurement campaigns. This database can be supplemented with measurements from the user to ensure compatibility with railway projects and enable hybrid predictions and transposition. Geographical and geotechnical data will be made importable through an interface with a GIS.

3 Numerical validation of the prediction tool

3.1 Problem outline

The numerical validation of the prediction tool is presented for a nominal InterCity (IC) train with 4 cars running at 50 km/h, 150 km/h and 300 km/h on a ballasted track (unevenness FRA class 6) supported by soft, medium and stiff soil.

The cars of the IC train are represented by a 10-DOF model, including the car body, two bogies, four wheelsets, as well as the primary and secondary suspensions (figure 3a). The train properties are summarized in table 1.

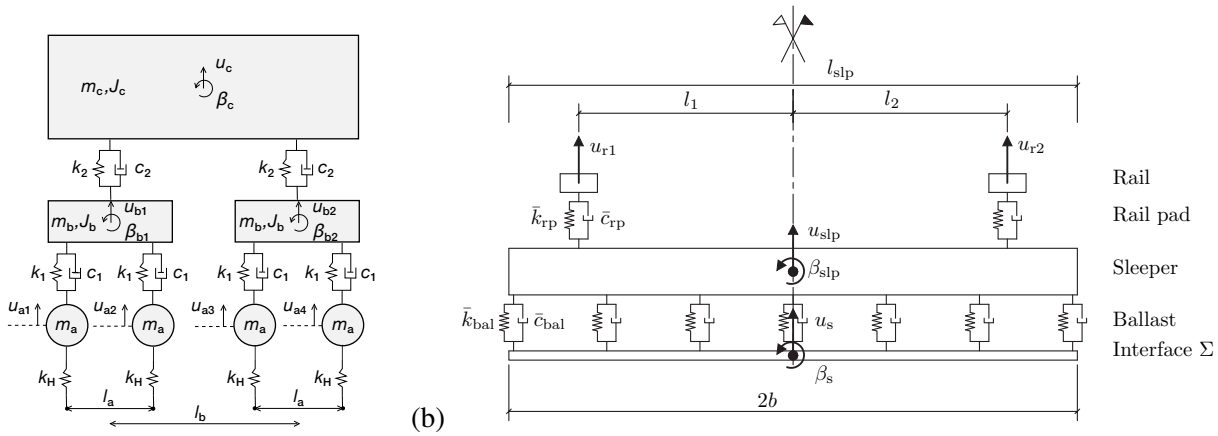

Figure 3: (a) 10-DOF model representing a car of the IC train and (b) cross-section of the ballasted track model.

Table 1: Properties of the IC train.

Car body	Vehicle length	$l_\mathrm{v} = 23$ m
	Mass	$m_\mathrm{c} = 32000$ kg
	Pitching moment of inertia	$J_\mathrm{cx} = 1.2 \times 10^6$ kgm^2
Bogie	Bogie spacing	$l_\mathrm{b} = 17$ m
	Mass	$m_\mathrm{b} = 5000$ kg
	Pitching moment of inertia	$J_\mathrm{bx} = 6000$ kgm^2
Wheelset (unsprung mass)	Axle spacing	$l_\mathrm{a} = 2.5$ m
	Mass	$m_\mathrm{a} = 1200$ kg
	Contact stiffness (per wheel)	$k_\mathrm{H} = 1.26 \times 10^9$ N/m
Primary suspension	Vertical stiffness per axle	$k_1 = 2 \times 10^6$ N/m
	Vertical viscous damping per axle	$c_1 = 40 \times 10^3$ Ns/m
Secondary suspension	Vertical stiffness per axle	$k_2 = 0.5 \times 10^6$ N/m
	Vertical viscous damping per axle	$c_2 = 31.6 \times 10^3$ Ns/m

The cross-section of the ballasted track model is shown in figure 3b and the track properties are summarized in table 2. The rails are modelled as Euler-Bernoulli beams with bending stiffness $E_{\mathrm{r}}I_{\mathrm{r}}$ and mass per unit length $\rho_{\mathrm{r}}A_{\mathrm{r}}$. The rail pads are modelled as continuous damped springs between the rails and the sleeper. The sleepers with mass m_{slp} are assumed to be rigid in the plane of the track cross-section. The ballast bed is modelled as a set of distributed, independent linear damped springs with stiffness per sleeper k_{bal} and mass per unit length m_{bal}. As 2.5D models are used, the equivalent stiffness per unit length is denoted by $\bar{k}_{\mathrm{rp}} = k_{\mathrm{rp}}/d$ for the rail pad and $\bar{k}_{\mathrm{bal}} = k_{\mathrm{bal}}/d$ for the ballast where d is the sleeper spacing.

Table 2: Properties of the ballasted track.

Rail UIC60	Rail positions	$l_1 = l_2 = 0.72$ m
	Cross-sectional area	$A_{\mathrm{r}} = 76.70 \times 10^{-4}$ m^2
	Moment of inertia about x-axis	$I_{\mathrm{r}} = 3057.1 \times 10^{-8}$ m^4
	Young's modulus	$E_{\mathrm{r}} = 210 \times 10^{9}$ N/m^2
	Damping loss factor	$\eta_{\mathrm{r}} = 0.01$
	Density	$\rho_{\mathrm{r}} = 7850$ kg/m^3
Rail pad	Stiffness	$k_{\mathrm{rp}} = 150 \times 10^{6}$ N/m
	Damping loss factor	$\eta_{\mathrm{rp}} = 0.3$
Sleeper	Spacing	$d = 0.6$ m
	Length	$l_{\mathrm{slp}} = 2.6$ m
	Height	$h_{\mathrm{slp}} = 0.2$ m
	Width	$b_{\mathrm{slp}} = 0.25$ m
	Mass	$m_{\mathrm{slp}} = 325$ kg
Ballast	Height	$h_{\mathrm{bal}} = 0.3$ m
	Top width	$b_{\mathrm{bal}t} = 3.0$ m
	Bottom width	$b_{\mathrm{bal}b} = 3.6$ m
	Stiffness per sleeper	$k_{\mathrm{bal}} = 500 \times 10^{6}$ N/m
	Poisson's ratio	$\nu_{\mathrm{bal}} = 0.0$
	Damping loss factor	$\eta_{\mathrm{bal}} = 0.15$
	Density	$\rho_{\mathrm{bal}} = 1500$ kg/m^3
	Mass per unit length	$m_{\mathrm{bal}} = 1485$ kg/m

The soil is characterized by its shear wave velocity C_{s}, dilatational wave velocity C_{p}, density ρ and material damping ratios β_{s} and β_{p} in shear and dilatational deformation, respectively. The dynamic soil characteristics of the three soil types used in the validation study are summarized in table 3.

Table 3: Dynamic soil characteristics.

Soil type	C_{s} [m/s]	C_{p} [m/s]	ρ [kg/m^3]	β_{s} [-]	β_{p} [-]
Soft	100	200	1800	0.025	0.025
Medium	200	400	1800	0.025	0.025
Stiff	400	800	1800	0.025	0.025

3.2 Modelling assumptions

Three modelling assumptions (labeled A1 to A3) are made in the prediction tool to reduce calculation times [14, 4]:

1. computation of the track compliance in a stationary instead of a moving frame of reference (A1);
2. application of the dynamic axle loads at fixed positions (low-speed approximation neglecting the Doppler effect) (A2);

3. incoherent instead of coherent axle loads (A3).

The influence of these assumptions is assessed by comparing the vibration velocity level predicted using TRAFFIC [2], a full model that accounts for moving loads and coherent axle loads, with the level predicted using the simplified model. The modelling assumptions are assessed step-by-step (A1 to A3) by means of a difference in vibration velocity level $\Delta \mathrm{L_v}(\mathbf{x}_1) = \mathrm{L_v^{approx}}(\mathbf{x}_1) - \mathrm{L_v^{ref}}(\mathbf{x}_1)$, where $\mathrm{L_v^{approx}}(\mathbf{x}_1)$ is the level accounting for a particular assumption and $\mathrm{L_v^{ref}}(\mathbf{x}_1)$ is the reference level (including any previous assumptions).

First, the effect of computing the track compliance in a stationary instead of a moving frame of reference is assessed (A1). Figure 4 shows that the vibration velocity level difference $\Delta \mathrm{L_v}(\mathbf{x}_1)$ is 1 dB or less for train speeds between 50 km/h and 300 km/h, regardless of the soil stiffness. Hence, the track compliance can, in very good approximation, be assessed in a stationary frame of reference when computing the dynamic axle loads, which results in a lower computational effort.

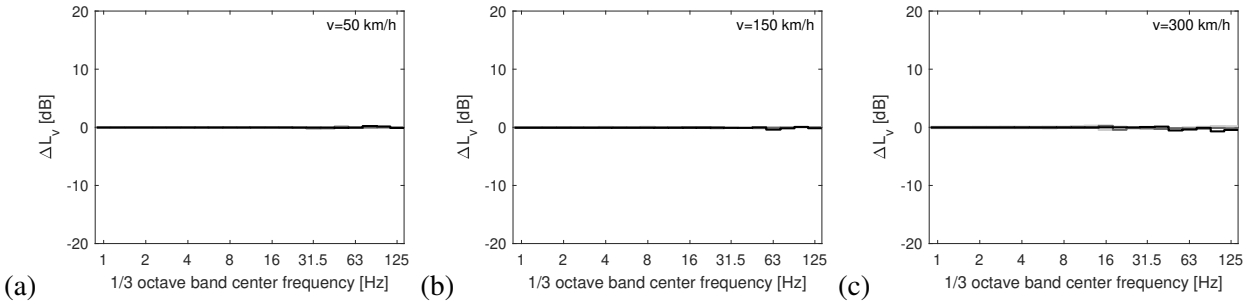

Figure 4: Vibration velocity level difference $\Delta \mathrm{L_v}(\mathbf{x}_1)$ when the track compliance is computed in the stationary frame of reference (A1) instead of the moving frame of reference. Results are shown at 16 m from the ballasted track on soft, medium and stiff soil (light to dark lines) for the IC train running at (a) 50 km/h, (b) 150 km/h and (c) 300 km/h.

The low-speed approximation (A2) predicts the stationary part of the response by assuming fixed axle positions. Figure 5 illustrates that, at 16 m from the track, the vibration level difference $\Delta \mathrm{L_v}(\mathbf{x}_1)$ increases with increasing train speed and is larger than 10 dB in individual frequency bands at high speed. The differences mainly correspond, however, to a redistribution of energy into different frequency bands because the Doppler effect is neglected. The overall vibration level summed over all bands is affected much less, with differences ranging from 2 to 3 dB [4, 14].

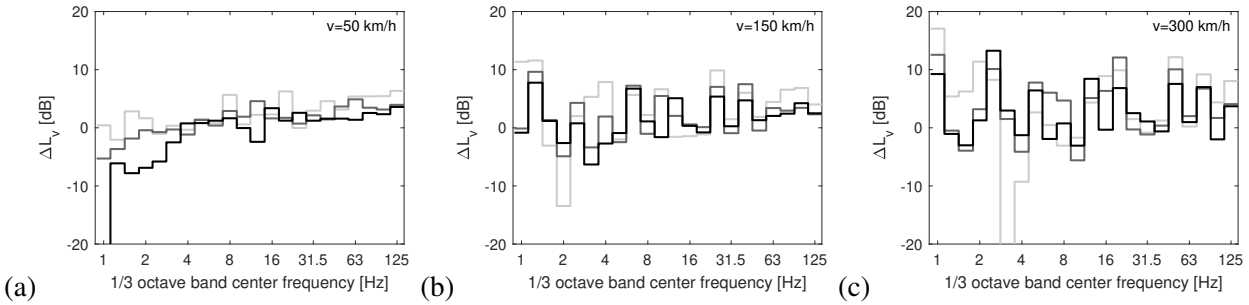

Figure 5: Vibration velocity level difference $\Delta \mathrm{L_v}(\mathbf{x}_1)$ between the low-speed approximation (A1 and A2) and the moving train response (A1). Results are shown at 16 m from the ballasted track on soft, medium and stiff soil (light to dark lines) for the IC train running at (a) 50 km/h, (b) 150 km/h and (c) 300 km/h.

Finally, the free field response is calculated assuming that the non-moving dynamic axle loads are incoherent (A3), whereas in the full model the wheels are assumed to be excited by the same unevenness apart from a time lag. Figure 6a shows that, at 16 m from the track, largest differences at 50 km/h occur below 4 Hz;

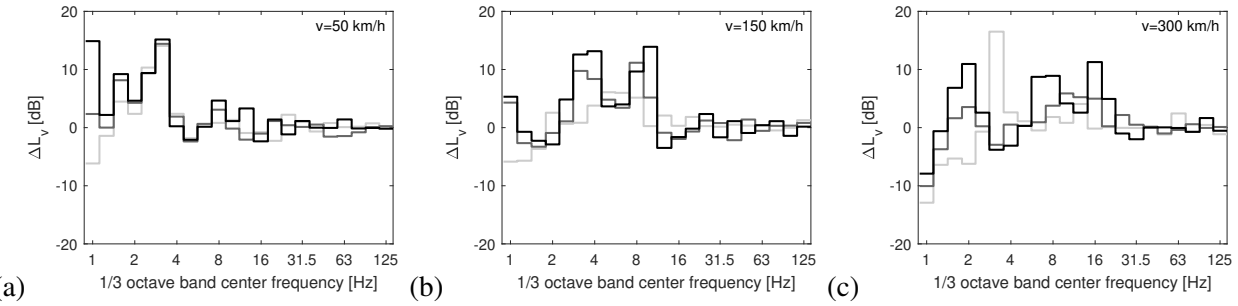

Figure 6: Vibration velocity level difference $\Delta \mathrm{L_v}(\mathbf{x}_1)$ between the assumption of incoherent (A1, A2 and A3) and coherent (A1 and A2) axle loads. Results are shown at 16 m from the ballasted track on soft, medium and stiff soil (light to dark lines) for the IC train running at (a) 50 km/h, (b) 150 km/h and (c) 300 km/h.

above 4 Hz, differences are less than 5 dB. At higher train speeds 150 km/h and 300 km/h (figures 6b-c), there is good agreement above 10 Hz and 20 Hz, respectively.

It is concluded that neglecting the Doppler effect has the largest influence on the vibration velocity level, whereas the assumption of incoherent axle loads mainly affects the response at low frequencies. The track compliance, however, can be computed in a stationary frame of reference as this does not significantly affect the predicted vibration velocity level.

The combined effect of all three assumptions on the vibration velocity level at 16 m from the track is shown in figure 7 for train speeds of 50 km/h, 150 km/h and 300 km/h. Although there are significant differences in individual frequency bands, the spectrum shape is closely followed. The smallest differences are observed for the IC train running at 50 km/h on the track supported by stiff soil. The overall vibration level summed over all frequency bands on average is 2 to 3 dB higher for the simplified model; consistent results were also found closer to and farther away from the track [4].

3.3 Comparison between the prediction tool and TRAFFIC

In order to validate its computational core, results obtained with the prediction tool are compared with TRAFFIC results (hereby accounting for the same modelling assumptions); as before, an IC train with 4 carriages running with a speed of 50 km/h, 150 km/h and 300 km/h on a ballasted track with unevenness class FRA 6 is considered. The contribution of the quasi-static axle loads is not included in the prediction tool, and is therefore also omitted in the calculations using TRAFFIC.

Since identical modelling assumptions are made in both models, a good agreement between results is expected. However, the prediction tool uses pre-computed soil impedance and transfer functions for an approximate track width of 3.0 m from its numerical database [15], while in TRAFFIC the actual track width of 3.6 m is used. This explains the slight discrepancies between the predictions with both models at high frequencies.

Figure 8 shows the line source transfer mobility $\mathrm{TM_L}(\mathbf{X}, \mathbf{x}_1)$ at 8 m, 16 m and 32 m from the ballasted track on soft, medium and stiff soil. At low frequencies, the line source transfer mobility is highest for the soft soil; the peak shifts to lower frequencies for increasing distance. At higher frequencies, the line source transfer mobility decreases due to material damping in the soil. For the medium and stiff soil, maximum response is observed at higher frequencies, while the effect of material damping is less pronounced. The results computed with the prediction tool and TRAFFIC are in excellent agreement up to 10 Hz. At higher frequencies, slightly higher values (1 to 3 dB) are obtained with the prediction tool due to the lower track width, with higher discrepancy at larger distance. Overall, the line source transfer mobility is in very good agreement, which demonstrates the correct modelling of the track-soil system in the prediction tool.

Figure 9 shows the vibration velocity level $\mathrm{L_v}(\mathbf{x}_1)$ at 16 m from the ballasted track (on soft, medium and stiff soil) during the passage of the IC train at three speeds. For a speed of 50 km/h, the velocity level is highest for the soft soil up to 30 Hz. For the medium and stiff soil, a maximum value is reached at the P2 resonance close

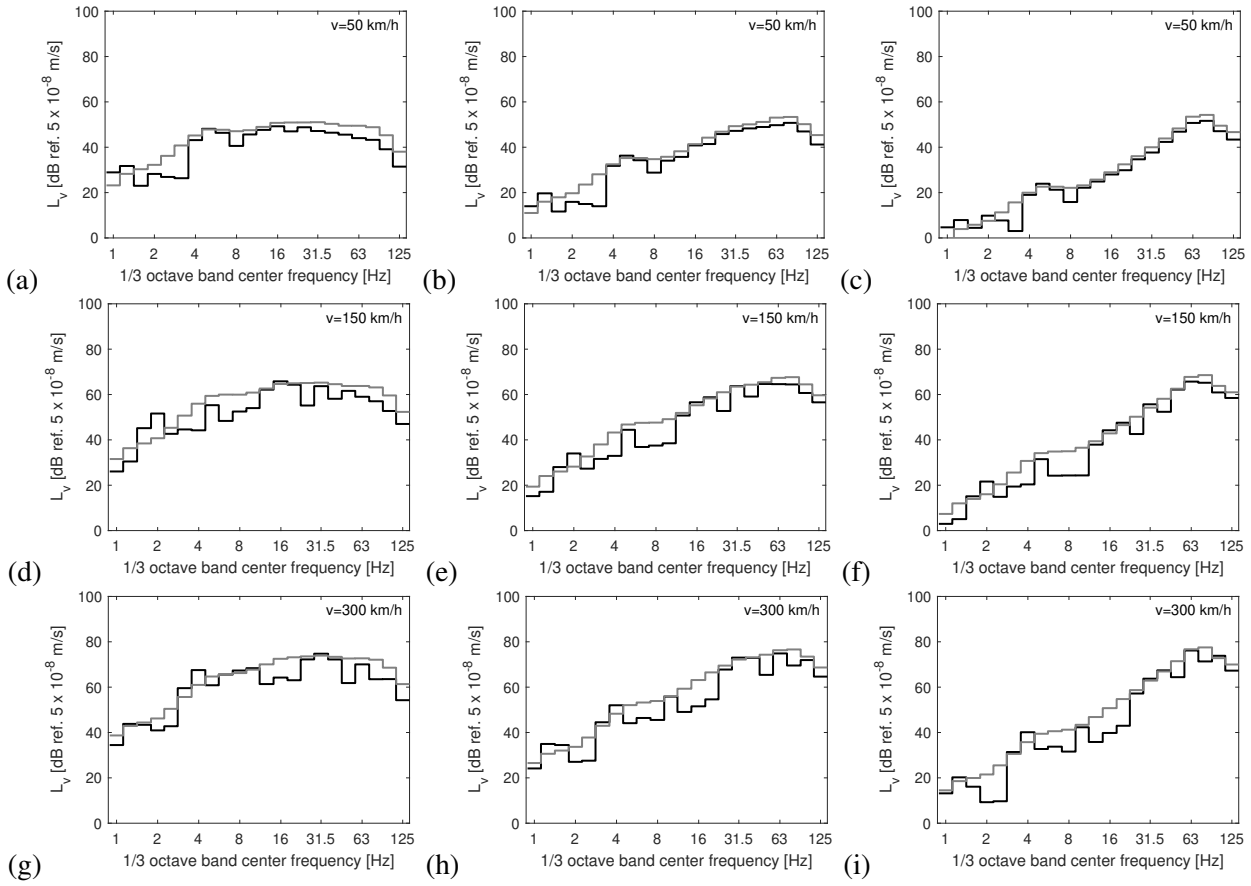

Figure 7: Vibration velocity level $\mathrm{L_v}(\mathbf{x}_1)$ at 16 m from the ballast track on (a,d,g) soft, (b,e,h) medium and (c,f,i) stiff soil for the IC train running at (a-c) 50 km/h, (d-f) 150 km/h and (g-i) 300 km/h. Results are computed with the full model (black line) and the simplified model (A1, A2 and A3; grey line).

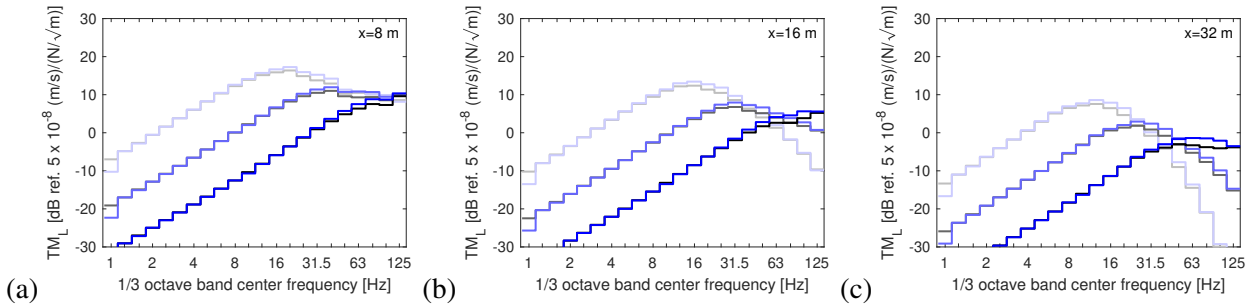

Figure 8: Line source transfer mobility $\mathrm{TM_L}(\mathbf{X}, \mathbf{x}_1)$ at (a) 8 m, (b) 16 m and (c) 32 m from the ballasted track on soft, medium and stiff soil (light to dark lines). Results are obtained with TRAFFIC (grey lines) and the prediction tool (blue lines).

to 80 Hz. Around this frequency, the velocity level is lower for the soft soil due to the influence of material damping. At higher train speeds, the velocity level increases, but the trends are very similar to those found at 50 km/h. Between 30 Hz and 125 Hz the velocity level increases by approximately 16 dB when increasing the train speed from 50 km/h to 150 km/h, independent of the soil stiffness. An additional increase of about 8 dB is observed by increasing the train speed to 300 km/h. Below 30 Hz, the velocity level predicted with TRAFFIC is 1 to 2 dB higher than with the prediction tool. At high frequencies, the tool tends to predict a slightly higher velocity level.

Figure 10 shows the force density $\mathrm{L_F}(\mathbf{X}, \mathbf{x}_1)$ based on the vibration velocity level and line source transfer mobility at 16 m from the track during the passage of the IC train at 50 km/h, 150 km/h and 300 km/h. Since

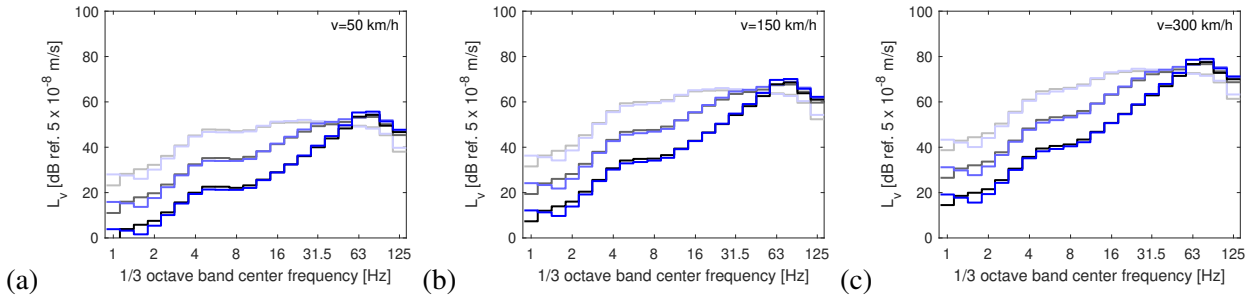

Figure 9: Vibration velocity level $L_v(\mathbf{x}_1)$ at 16 m from the ballasted track on soft, medium and stiff soil (light to dark lines) for the IC train running at (a) 50 km/h, (b) 150 km/h and (c) 300 km/h. Results are obtained with TRAFFIC (grey lines) and the prediction tool (blue lines).

the influence of the soil stiffness on the dynamic axle loads is limited below 50 Hz, the force density is almost identical for the three soil types up to this frequency. At high frequencies, the force density is higher for the soft soil. The force density increases with increasing train speed in a similar way to the vibration velocity level (figure 9). The force densities computed with the prediction tool and TRAFFIC are in very good agreement. The discrepancy is limited to 3 dB in each frequency band and is due to the different track width when pre-computing the soil impedance and transfer functions.

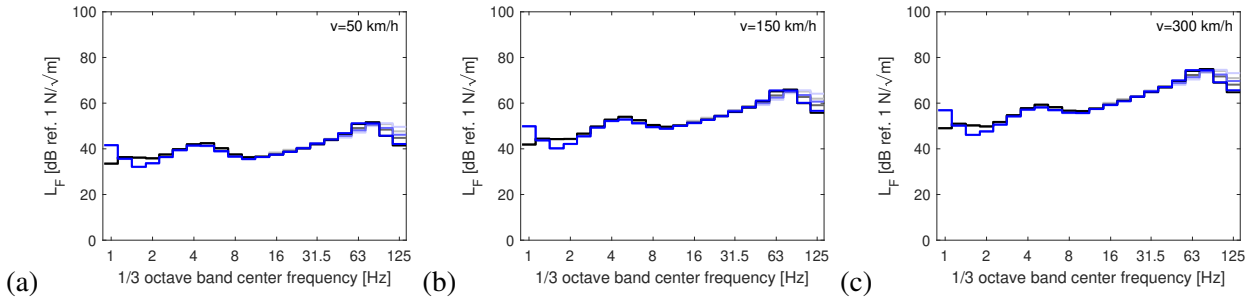

Figure 10: Force density $L_F(\mathbf{X}, \mathbf{x}_1)$ at 16 m from the ballasted track on soft, medium and stiff soil (light to dark lines) for the IC train running at (a) 50 km/h, (b) 150 km/h and (c) 300 km/h. Results are obtained with TRAFFIC (grey lines) and the prediction tool (blue lines).

4 Experimental validation of the prediction tool

4.1 Case description

An extensive measurement campaign [16, 17, 18] was carried out at a site in Lincent (Belgium) on the high speed line L2 connecting Brussels and Köln. This experimental case history is identified as a benchmark to be included in the hybrid prediction tool. Transfer functions between the track and the free field and vibration measurements during train passages (InterCity, ICE and Thalys) were processed (in terms of vibration levels and line source transfer mobilities) to ensure compatibility with the hybrid prediction tool.

A cross-section of the site is shown in figure 11. The high speed line L2 consists of two railway tracks, one track in the direction of Liège (track 1) and one track in the direction of Brussels (track 2). The ballasted track consists of two UIC 60 rails supported every 0.6 m by rubber pads on monoblock concrete sleepers. The track gauge equals 1.435 m. The track properties are summarized in table 4. The track unevenness was measured, and the measured data are reliable for wavelengths between 3 m and 63 m.

In situ tests were performed at the site in Lincent for the identification of the (small strain) dynamic soil characteristics, including Seismic Cone Penetration Tests (SCPTs), Spectral Analysis of Surface Waves (SASW) tests and Seismic Refraction (SR) tests. Table 5 presents the dynamic soil characteristics at the Lincent site.

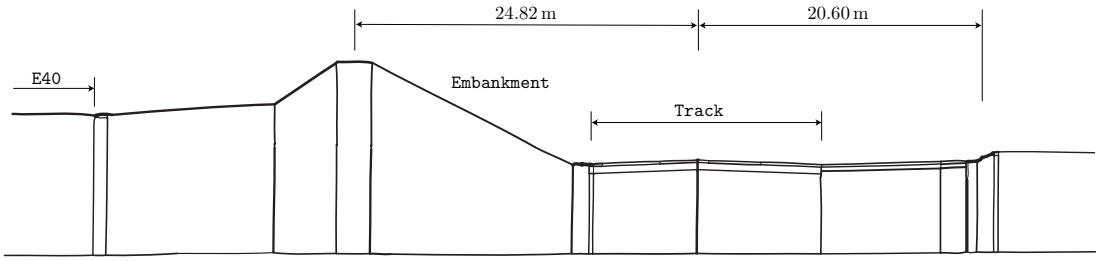

Figure 11: Cross-section of the measurement site in Lincent.

Table 4: Track properties for the Lincent site.

UIC60 rail	Rail positions	$l_1 = l_2 = 0.72$ m
	Bending stiffness	$E_\mathrm{r} I_\mathrm{r} = 6.42 \times 10^6$ Nm^2
	Mass per unit length	$\rho_\mathrm{r} A_\mathrm{r} = 60$ kg/m
Rail pad	Stiffness	$k_\mathrm{rp} = 153.4 \times 10^6$ N/m
	Viscous damping coefficient	$c_\mathrm{rp} = 13.5 \times 10^3$ Ns/m
Sleeper	Length	$l_\mathrm{slp} = 2.5$ m
	Width	$b_\mathrm{slp} = 0.235$ m
	Height	$h_\mathrm{slp} = 0.205$ m
	Mass	$m_\mathrm{slp} = 300$ kg
	Mass moment of inertia	$\rho I_\mathrm{t,slp} = 157.3$ kgm^2
	Spacing	$d = 0.6$ m
Ballast	Thickness	$t_\mathrm{bal} = 0.35$ m
	Top width	$b_\mathrm{bal}t = 3.6$ m
	Bottom width	$b_\mathrm{bal}b = 5.6$ m
	Mass per unit length	$m_\mathrm{bal} = 1488$ kg/m
	Stiffness per sleeper	$k_\mathrm{bal} = 180 \times 10^6$ N/m
	Hysteretic loss factor	$\eta_\mathrm{bal} = 0.06$
Subgrade	Thickness	$t_\mathrm{sub} = 1.0$ m
	Shear wave velocity	$C_\mathrm{s,sub} = 300$ m/s
	Density	$\rho_\mathrm{sub} = 1854$ kg/m^3

The experimental validation is performed for 26 passages of an IC-A train consisting of 1 locomotive HLE 13, 11 standard carriages I11 and 1 end carriage I11 BDx with a total length $L_\mathrm{t} = 335.91$ m (from first to last axle). Each locomotive and carriage has two independent bogies and four axles. The vehicle length l_v, the bogie spacing l_b, the axle spacing l_a, the total mass per axle m_t, the sprung mass m_s and the unsprung mass m_u of all cars are summarized in table 6. A 1-DOF model is used to represent the individual wheelsets. The average train speed for the 26 passages is around 198 km/h.

4.2 Comparison with the prediction tool

Figure 12 plots the measured line source transfer mobility $\mathrm{TM_L}(\mathbf{X}, \mathbf{x}_1)$ at 12 m, 32 m and 64 m from the track (black line) due to impacts at the sleeper edge (eccentricity of 1.1 m). In the prediction tool, however, impacts at both rails are considered. Hence, the measured data are modified by adding a correction factor that accounts for the position of the source points (grey line). Good agreement is obtained between the experimental data and the predictions (blue line) in the frequency range between 12.5 Hz and 40 Hz. Below 8 Hz, the measured values are quite high due to low frequency measurement noise. Above 40 Hz, the simulated values are generally lower than the measured values. The best agreement is observed at 32 m. At 64 m, the simulated values are about 10 dB lower than the measured values, possibly due to overestimated soil damping in the model.

Table 5: Dynamic soil characteristics at the Lincent site.

Layer	h [m]	C_s [m/s]	C_p [m/s]	β_s [-]	β_p [-]	ρ [kg/m^3]
1	1.4	128	286	0.044	0.044	1800
2	2.7	176	286	0.038	0.038	1800
3	∞	355	1667	0.037	0.037	1800

Table 6: Geometrical and mass properties of the IC-A train [16, 19]: vehicle length l_v, bogie spacing l_b, axle spacing l_a, total mass m_t, sprung mass m_s and unsprung mass m_u.

	Number of axles	l_v [m]	l_b [m]	l_a [m]	m_t [kg]	m_s [kg]	m_u [kg]
Locomotive	4	19.11	10.40	3.00	22500	19677	2823
Central carriage	4	26.40	18.40	2.56	11610	10100	1500
End carriage	4	26.40	18.40	2.56	11830	10286	1544

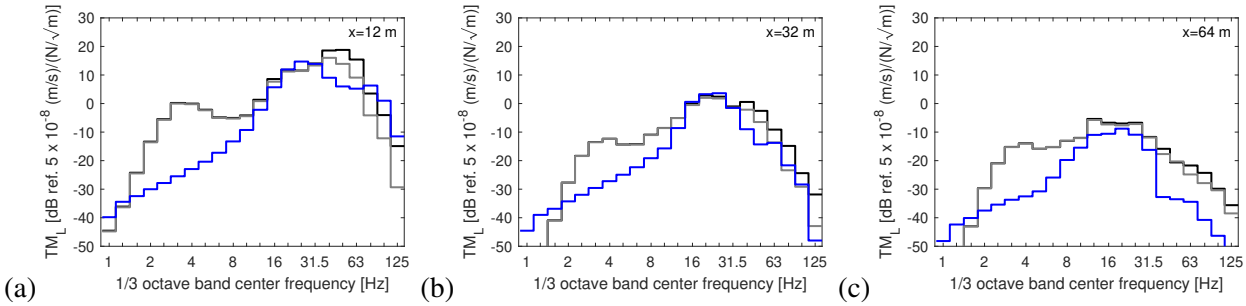

Figure 12: Line source transfer mobility $\mathrm{TM_L}(\mathbf{X}, \mathbf{x}_1)$ for receivers at (a) 12 m, (b) 32 m and (c) 64 m from the track at Lincent. Experimental data are shown for source points at the sleeper edge (black line). The experimental data are corrected to account for the position of the source points (grey line) and are compared to results obtained with the prediction tool (blue line).

Figure 13 shows the mean (black line) and two standard deviation range (grey lines) of the measured vibration velocity level during 26 passages of the IC-A train in a speed range between 178 km/h and 218 km/h. The uncertainty on the vibration velocity level is high below 10 Hz due to low frequency measurement noise. Around 50 Hz, the numerical and the experimental data show a peak related to the P2 (unsprung mass) resonance; this peak is less pronounced at 64 m due to the effect of material and geometrical damping in the soil. A peak is observed at 20 Hz corresponding to the axle passage frequency. The quasi-static contribution is observed below 8 Hz close to the track; it is not included in the predictions with the prediction tool. The coach and bogie suspension modes, which influence the response at low frequencies, are also not observed in the predictions because a 1-DOF vehicle model is used.

Good agreement is observed between the measured and predicted vibration velocity level between 10 Hz and 40 Hz. At higher frequencies, the predicted vibration velocity level is lower than the measured data, which is consistent with observations for the $\mathrm{TM_L}(\mathbf{X}, \mathbf{x}_1)$ (figure 12). Furthermore, it should be noted that the track unevenness is extrapolated for wavelengths shorter than 3 m, corresponding to frequencies above 18.3 Hz for the considered train speed, which causes additional uncertainty. Although significant differences are observed between the measured data and the predicted levels in some frequency bands, table 7 shows that the discrepancy between the global vibration levels $\mathrm{L_v^{global}}(\mathbf{x}_1)$ is less than 2 dB.

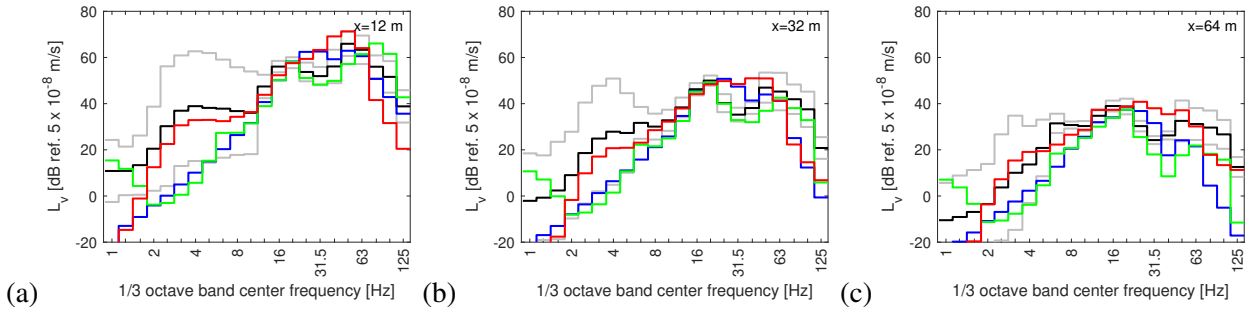

Figure 13: Vibration velocity level $\mathrm{L_v}(\mathbf{x}_1)$ for receivers at (a) 12 m, (b) 32 m and (c) 64 m from the track at Lincent for 26 passages of the IC-A train in a speed range between 178 km/ and 218 km/h: mean (black line) and two standard deviation (2σ) range (grey lines). The vibration velocity level is also calculated with the prediction tool for a train speed of 198 km/h: fully numerical (blue line), hybrid model 1 (red line) and hybrid model 2 (green line).

5 Hybrid predictions

The hybrid prediction schemes introduced in section 2.4 are also demonstrated for the site in Lincent. Figure 13 compares the experimental data to the hybrid and fully numerical predictions for the IC-A train. Hybrid model 1 (predicted force density and measured line source transfer mobility) overestimates the vibration velocity level around the P2 resonance at 50 Hz. This is due to the fact the unevenness in this frequency range was not measured. Hybrid model 2 (measured force density and predicted line source transfer mobility) gives better agreement with measurements, especially at 32 m.

Table 7 summarizes the measured and predicted global vibration velocity levels. Hybrid model 1 gives the largest discrepancies compared to measurements, with differences of up to 5 dB. The fully numerical model and hybrid model 2 give differences of 1 to 2 dB compared to the measured data. These differences are acceptable for numerical predictions, given the model and parameter uncertainty.

Table 7: Measured and predicted global vibration velocity level $\mathrm{L_v^{global}}(\mathbf{x}_1)$ [dB ref. 5×10^{-8} m/s] at 12 m, 32 m and 64 m from the track at Lincent during the passage of the IC-A train running at 198 km/h.

Receiver location x	12 m	32 m	64 m
Measured (mean - 2σ)	64.3	50.7	41.3
Measured (mean)	69.3	54.5	44.5
Measured (mean + 2σ)	75.5	60.4	49.0
Fully numerical prediction	69.3	55.3	42.3
Prediction with hybrid model 1	74.5	57.3	46.8
Prediction with hybrid model 2	69.3	52.1	40.0

6 Conclusion

The proposed modular approach for the vibration prediction tool provides full modelling flexibility at each stage of the design process. Embedding it in existing software simplifies the modelling process, as fewer interfaces are needed. Extensive validation and approval testing increases confidence levels.

The modelling assumptions made in the prediction tool were validated with TRAFFIC. It is concluded that the low-speed approximation leads to a redistribution of energy in frequency bands, but that the global vibration velocity level only differs by 2 to 3 dB compared with results obtained for moving loads. Additionally, the assumption of incoherent axle loads does not significantly affect the vibration velocity level above 10 Hz.

Subsequently, the computational core of the prediction tool was validated with TRAFFIC for a number of numerical case histories. Good agreement is found for the line source transfer mobility, vibration velocity level and force density.

Measured data at a site in Lincent were used for the experimental validation of the prediction tool, and to demonstrate the hybrid prediction schemes implemented in the tool. Although significant differences are observed in the spectrum shape of the predicted and measured vibration velocity level due to unknown track unevenness at small wavelengths and possible overestimation of the material damping in the soil, the global vibration velocity level averaged over all frequency bands agrees well.

Once finalized, the vibration prediction tool will enable the assessment of vibration levels for both large-scale studies and more detailed investigations for new and upgraded railway lines.

Acknowledgements

The results presented in this paper have been obtained within the frame of the project SILVARSTAR ”Soil vibration and Auralisation Software Tools for Application in Railways”. This project has received funding from the Shift2Rail Joint Undertaking (JU) under Grant Agreement 101015442. The JU receives support from the European Union’s Horizon 2020 Research and Innovation Programme and the Shift2Rail JU members other than the Union. The financial support is gratefully acknowledged.

References

[1] G. Degrande, G. Lombaert, E. Ntotsios, D. Thompson, B. Nélain, P. Bouvet, S. Grabau, J. Blaul, and A. Nuber, “State-of-the-art and concept of the vibration prediction tool,” SILVARSTAR project GA 101015442, Deliverable D1.1, Report to the EC, May 2021.

[2] G. Lombaert, S. François, and G. Degrande, “TRAFFIC Matlab toolbox for traffic induced vibrations,” Department of Civil Engineering, KU Leuven, Report BWM-2012-10, November 2012, user’s Guide Traffic 5.2.

[3] *ISO 14837-1:2005 Mechanical vibration - Ground-borne noise and vibration arising from rail systems - Part 1: General guidance*, International Organization for Standardization, 2005.

[4] P. Reumers, G. Degrande, G. Lombaert, F. Seyfaddini, G. Herremans, E. Ntotsios, D. Thompson, B. Nélain, P. Bouvet, B. Fröhling, and A. Nuber, “Validation of the prototype vibration prediction tool against documented cases,” SILVARSTAR project GA 101015442, Deliverable D1.3, Report to the EC, June 2022.

[5] C. Hanson, J. Ross, and D. Towers, “High-Speed Ground Transportation Noise and Vibration Impact Assessment,” U.S. Department of Transportation, Federal Railroad Administration, Office of Railroad Policy and Development, Tech. Rep. DOT/FRA/ORD-12/15, September 2012.

[6] A. Quagliata, M. Ahearn, E. Boeker, C. Roof, L. Meister, and H. Singleton, “Transit Noise and Vibration Impact Assessment Manual,” U.S. Department of Transportation, Federal Transit Administration, John A. Volpe National Transportation Systems Center, FTA 0123, September 2018.

[7] M. Villot, C. Guigou, P. Jean, and N. Picard, “Procedures to predict exposure in buildings and estimate annoyance,” RIVAS project SCP0-GA-2010-265754, Deliverable D1.6, Report to the EC, 2012.

[8] D. Stiebel, H. Brick, R. Garburg, G. Schleinzer, H. Zandberg, B. Faure, A. Pfeil, S. Thomas, A. Guiral, and M. Oregui, “Specification of model requirements including descriptors for vibration evaluation,” FINE2 project GA-881791, Deliverable D8.1, Report to the EC, 2020.

[9] B. Nélain, N. Vincent, and E. Reynaud, "Towards hybrid models for the prediction of railway induced vibration: numerical verification of two methodologies," in *Proceedings of the 13th International Workshop on Railway Noise, IWRN13*, G. Degrande and G. Lombaert, Eds., Ghent, Belgium, September 2019, pp. 1–8.

[10] E. Ntotsios, D. Thompson, and M. Hussein, "The effect of track load correlation on ground-borne vibration from railways," *Journal of Sound and Vibration*, vol. 402, pp. 142–163, 2017.

[11] E. Ntotsios, D. Thompson, and M. Hussein, "A comparison of ground vibration due to ballasted and slab tracks," *Transportation Geotechnics*, vol. 21, no. 100256, 2019.

[12] P. Galvín, S. François, M. Schevenels, E. Bongini, G. Degrande, and G. Lombaert, "A 2.5D coupled FE-BE model for the prediction of railway induced vibrations," *Soil Dynamics and Earthquake Engineering*, vol. 30, no. 12, pp. 1500–1512, 2010. [Online]. Available: http://dx.doi.org/10.1016/j.soildyn.2010.07.001

[13] D. Thompson, E. Ntotsios, G. Degrande, G. Lombaert, G. Herremans, T. Alexiou, B. Nélain, S. Barcet, P. Bouvet, B. Fröhling, and A. Nuber, "Database for vibration emission, ground transmission and building transfer functions," SILVARSTAR project GA 101015442, Deliverable D2.1, Report to the EC, January 2022.

[14] D. Thompson, E. Ntotsios, P. Bouvet, B. Nélain, S. Barcet, A. Nuber, B. Fröhling, P. Reumers, F. Seyfaddini, G. Herremans, G. Lombaert, and G. Degrande, "The influence of model assumptions in a hybrid prediction tool for railway induced vibration," in *Proceedings of the 51st International Congress and Exposition on Noise Control Engineering, Inter-Noise 2022*, Glasgow, United Kingdom, August 2022.

[15] S. Barcet, B. Nélain, P. Bouvet, D. Thompson, E. Ntotsios, G. Degrande, G. Lombaert, B. Fröhling, and A. Nuber, "Description of the vibration prediction tool," SILVARSTAR project GA 101015442, Deliverable D1.2, Report to the EC, June 2022.

[16] H. Verbraken, "Prediction of railway induced vibration by means of numerical, empirical, and hybrid methods," Ph.D. dissertation, Department of Civil Engineering, KU Leuven, 2013.

[17] H. Verbraken, G. Degrande, G. Lombaert, B. Stallaert, and V. Cuéllar, "Benchmark tests for soil properties, including recommendations for standards and guidelines," RIVAS project SCP0-GA-2010-265754, Deliverable D1.11, Report to the EC, December 2013.

[18] H. Verbraken, P. Coulier, G. Lombaert, and G. Degrande, "Measurement of train passages and transfer functions at a site in Lincent," Department of Civil Engineering, KU Leuven, Report BWM-2012-05, June 2012.

[19] G. Lombaert and G. Degrande, "Ground-borne vibration due to static and dynamic axle loads of InterCity and high speed trains," *Journal of Sound and Vibration*, vol. 319, no. 3-5, pp. 1036–1066, 2009. [Online]. Available: http://dx.doi.org/10.1016/j.jsv.2008.07.003

Appendix

A Disclaimer

The information in this document is provided "as is" and no guarantee or warranty is given that the information is fit for any particular purpose. The content of this document reflects only the authors' view - the Shift2Rail Joint Undertaking is not responsible for any use that may be made of the information it contains. The users use the information at their sole risk and liability.